Electronic - Supplementary Materials

C Journal of Carbon Research

Characterization of molecular spacer enhanced nanostructured carbons for electrical energy storage

Justin A. Zuczek,[a] Matthew Bonfield,[a] Nesreen Elathram,[a] William R. Hixson,[a] Terawit Kongruengkit[a], James B. Mitchell,[a] Nickolas Zelenka,[a] Leonid D. Popov,[b] Andrey Morozov[b], Igor N. Shcherbakov,[b] and J. C. Poler[a†]

[a] Department of Chemistry, University of North Carolina at Charlotte, Charlotte, NC
[b] Chair of Physical and Colloid Chemistry, Southern Federal University, Rostov -on -Don, Russian Federation.

[a†] Corresponding Author: Department of Chemistry, University of North Carolina at Charlotte, Charlotte, NC Fax: (704) 687-0960; Tel: (704) 687-8289; E-mail: jcpoler@uncc.edu

LIST OF ABBREVIATIONS

+2Cu2	4-(*tert*-butyl)-2,6-bis((2-(phthalazin-1-yl)hydrazono)methyl) phenol(m_2-methoxo) dicopper(II)-chloride
+2Cu2FcOH	biscopper [4-*tert*-butyl-2,6-diformylphenol bis-ferrocenoylhydrazone hydroxide]-(NO3)2
+2Ru2	[Cl(2,20;60,200-terpyridine)Ru(tetrapyrido-[3,2-a:20,30 c:300,200h:200,300j]phenazine)Ru(2,20;60,200-terpyridine)Cl]-(PF6)2
+2Zn2	4-(*tert*-butyl)-2,6-bis((2-(phthalazin-1-yl)hydrazono)methyl) phenol(m_2-methoxo) dizinc(II)-acetate
+2Zn2Ac	4-(*tert*-butyl)-2,6-bis((2-(phthalazin-1-yl)hydrazono)methyl) phenol (m_2-methoxo acetate) dizinc(II)-acetate
AcFc	acetylferrocene
AFM	atomic force microscopy
$Ag/AgNO_3$	silver/silver nitrate

AIC	Akaike's information criterion
ATR FT-IR	attenuated total reflection Fourier-transform infrared spectroscopy
CCC	critical coagulation concentration
CE	counter electrode
CHI_3	iodoform
CNI	carbon nanotechnologies inc. SWCNTs
CNTs	carbon nanotubes
Cu2FcCl3	biscopper [4-*tert*-butyl-2,6-diformylphenol bis-ferrocenoylhydrazone trichloride]
Cu2FcOH	biscopper [4-*tert*-butyl-2,6-diformylphenol bis-ferrocenoylhydrazone hydroxide]
$Cu(NO_3)_2$	copper (ii) nitrate
C_S	specific capacitance
CV	cyclic voltammetry
DFT	density functional theory
DLA	diffusion limited aggregation
DMF	N,N-dimethylformamide
DMSO	dimethyl sulfoxide
D_S	dispersion stability
EDL	electrical double layer
EDLC	electrical double layer capacitor
EDX	energy dispersive x-ray spectroscopy
EELS	electron energy loss spectroscopy
EIS	electrochemical impedance spectroscopy
EtOH	ethanol
GCD	galvanostatic charge-discharge
HCl	hydrochloric acid
HiPco	high pressure carbon monoxide
HOMO	highest occupied molecular orbital
IASS	ion-accessible surface site

ILCT	ion-ligand charge transfer
IPA	isopropyl alcohol
ITO	indium tin oxide
LUMO	lowest unoccupied molecular orbital
MeCN	acetonitrile
MeOH	methanol
MLCT	metal-ligand charge transfer
MOF	metal organic framework
MS	mass spectrometry
MWCNTs	multi-walled carbon nanotubes
NaBr	sodium bromide
NaOH	sodium hydroxide
NI	NanoIntegris SWCNTs
NMP	N-methyl-2-pyrrolidone
PPr	polypropylene
PTFE	polytetrafluoroethylene
RBF	round bottom flask
RE	reference electrode
RLA	reaction limited aggregation
RMS	root mean squared
SC	supercapacitor
SHE	standard hydrogen electrode
SSA	specific surface area
SWCNTs	single-walled carbon nanotubes
TBATFB	tetrabutylammonium tetrafluoroborate
^{t}Bu	tert-butyl
TD-DFT	time dependent density functional theory
TsOH	p-toluene sulfonic acid

UV-Vis-NIR ultraviolet-visible-near infrared

WE working electrode

Molecular Spacers

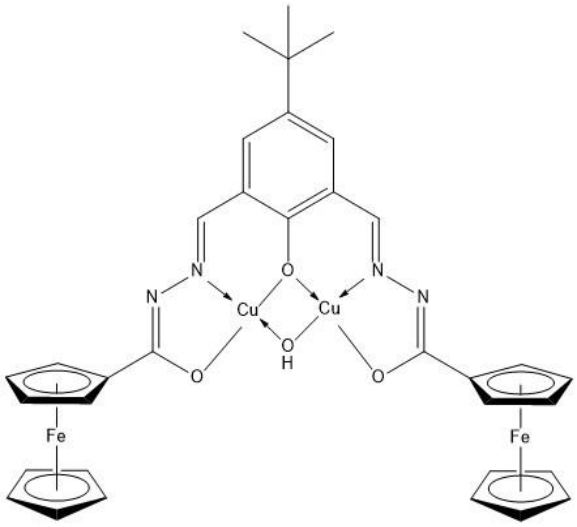

Figure S1: Confirmed structure of Cu2FcOH. Ferrocene ligands provide redox sites, aromaticity provides binding to SWCNTs, and ^{t}Bu provides steric bulk.

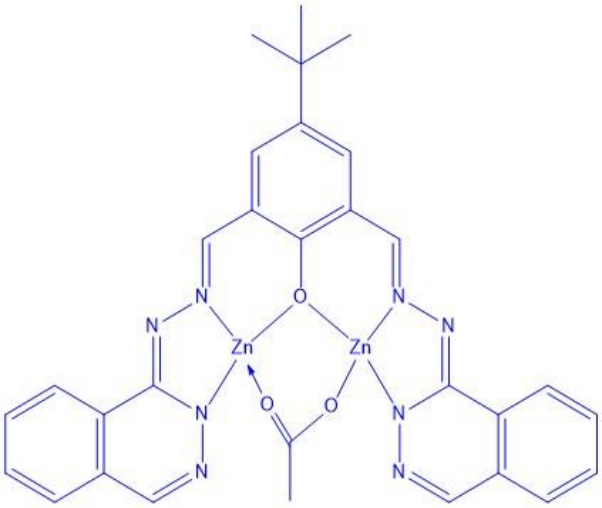

Figure S2: Structure of +2Zn2Ac. Added aromaticity should provide strong binding to SWCNTs, and the ^{t}Bu provides steric bulk.

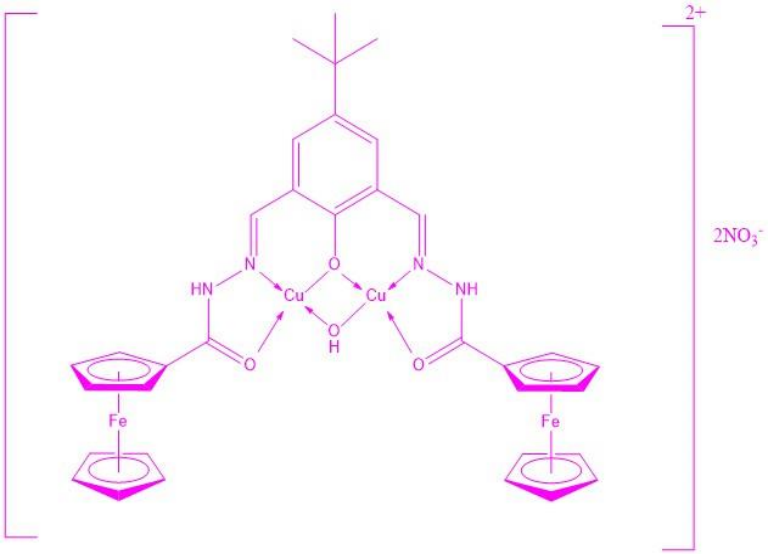

Figure S3: Structure of +2Cu2FcOH. Ferrocene ligands provide redox sites, aromaticity provides binding to SWCNTs, and ^{t}Bu provides steric bulk. The dication overall charge should provide stronger binding via electrostatic interactions compared to Cu2FcOH.

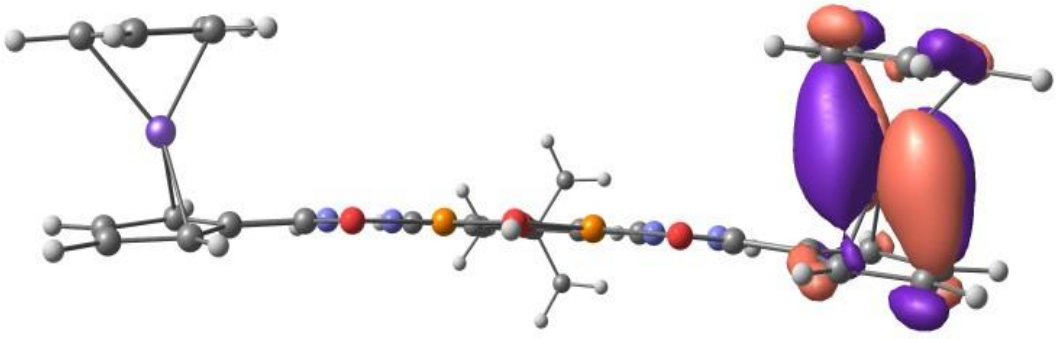

Figure S4: Calculated HOMO for +2Cu2FcOH looking down the Z-axis.

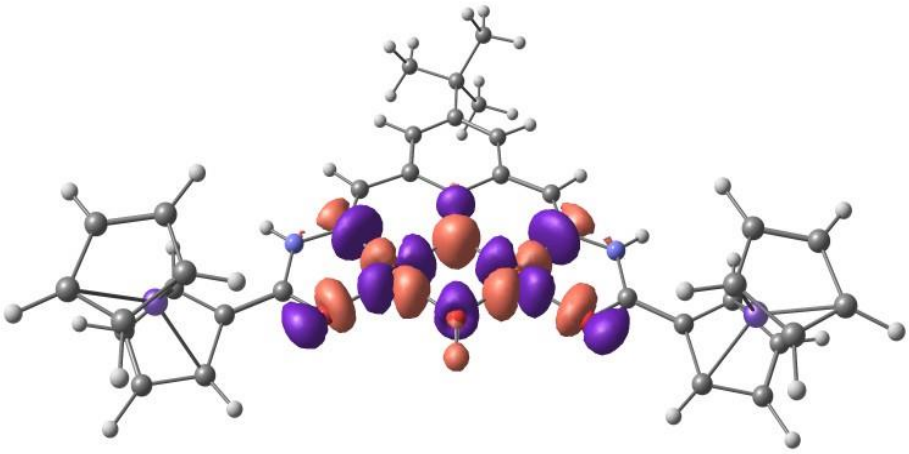

Figure S5: Calculated LUMO for +2Cu2FcOH.

		Energy (eV)
αHOMO	Ferrocene ligand	-0.3764
αHOMO	Second ferrocene ligand	-0.3759
βHOMO	Ferrocene ligand	-0.3763
βHOMO	Second ferrocene ligand	-0.3758
αLUMO	Copper and bridge	-0.2871
αLUMO	Copper and bridge	-0.2801
βLUMO	Copper and bridge	-0.3282
βLUMO	Copper and bridge	-0.3055

Table S1: Calculated HOMO and LUMO energies for +2Cu2FcOH. ΔV of 0.09 V measured between HOMO and LUMO (α). For the ligand, measured energy difference was 3.8 V, a 97.6% decrease. Optical transitions from absorption spectroscopy between the HOMO and LUMO would be unmeasurable.

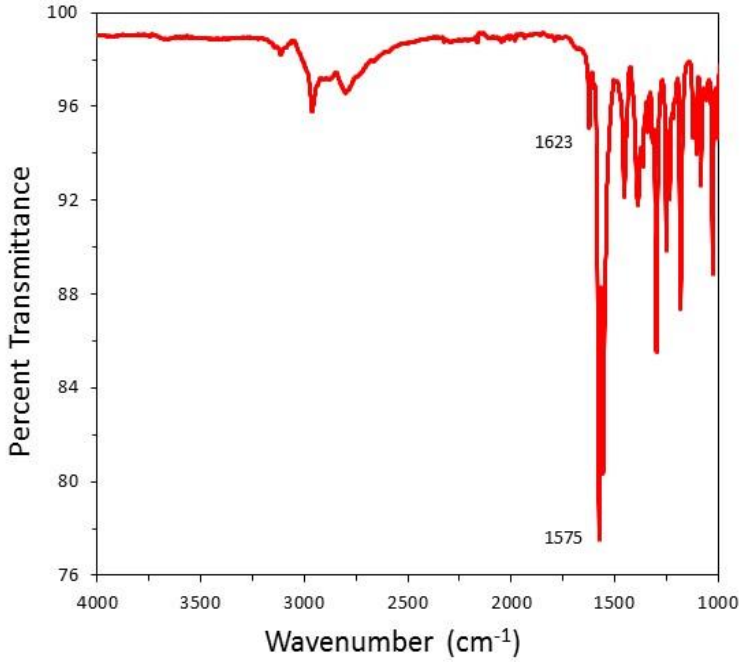

Figure S6: IR spectra of Cu2FcCl3. -C=O (1623 cm^{-1}), -C=N (1575 cm^{-1}). Ferrocene vibrates around 480 cm^{-1}.

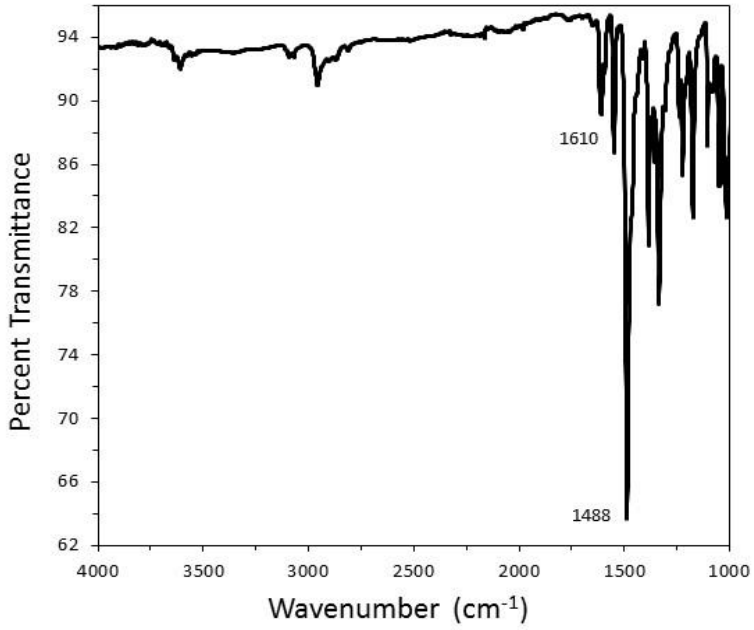

Figure S7: IR spectra of Cu2FcOH. -C=N (1610 cm^{-1}), -C=C (1488 cm^{-1}). Ferrocene vibrates around 480 cm^{-1}.

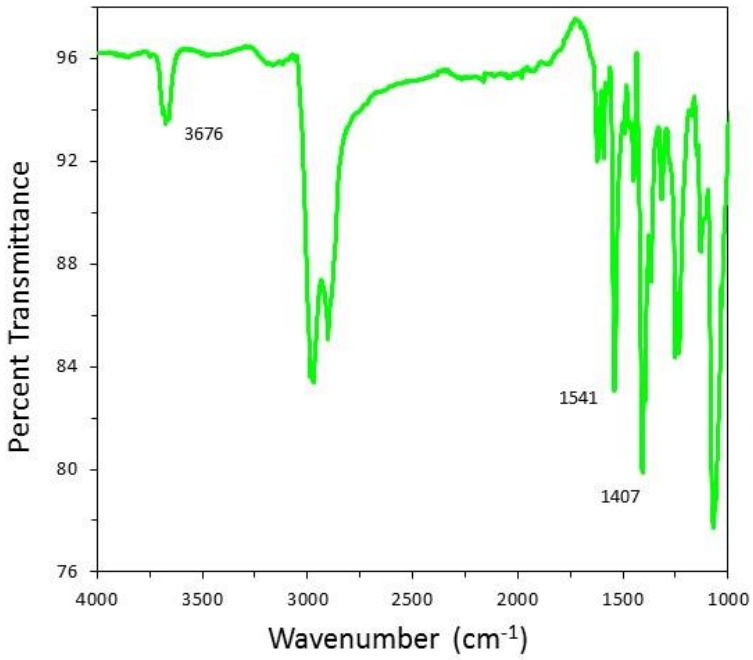

Figure S8: IR spectra of +2Cu2. Unidentified (3676 cm^{-1}), -C=N (1541 cm^{-1}), -C=C (1407 cm^{-1}).

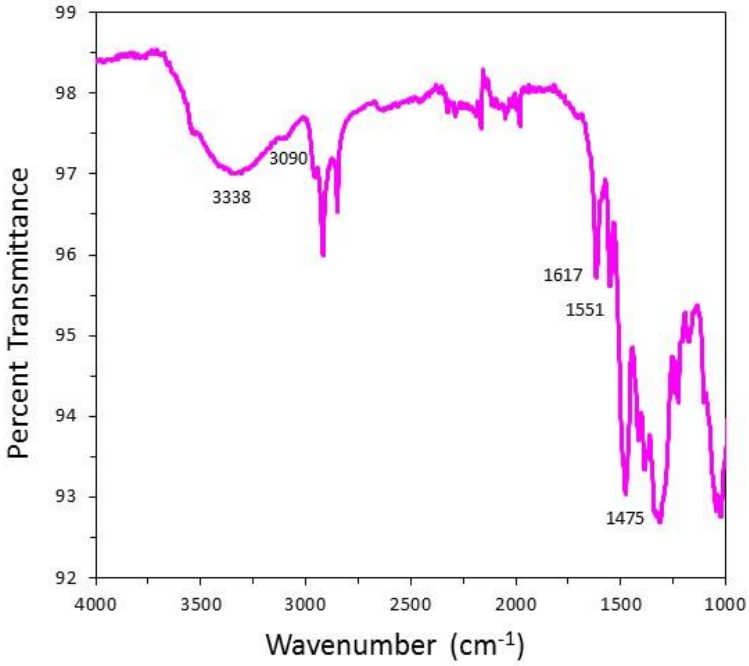

Figure S9: IR spectra of +2Cu2FcOH. –O-H (3338 cm^{-1}), -N-H (3090 cm^{-1}), -C=O (1617 cm^{-1}), -C=N (1551 cm^{-1}), -C=C (1475 cm^{-1}). Ferrocene vibrates around 480 cm^{-1}.

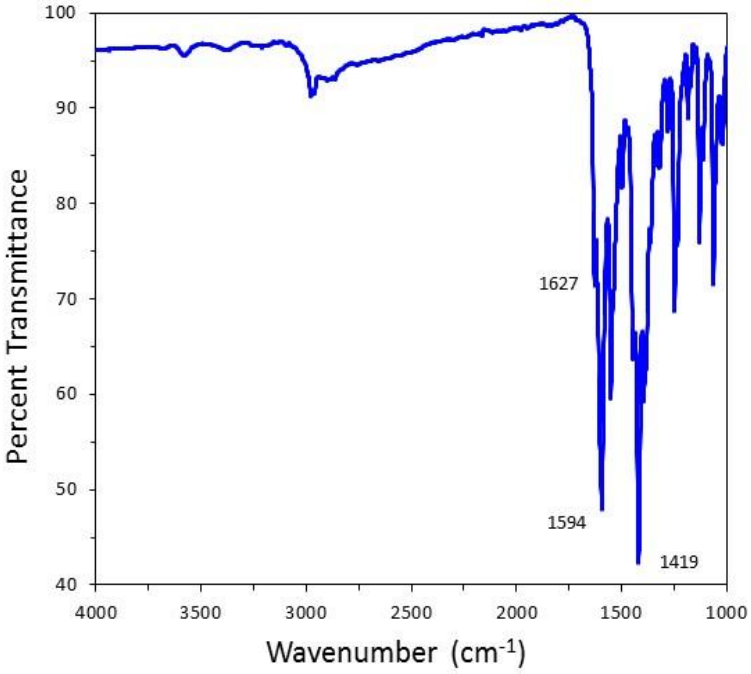

Figure S10: IR spectra of +2Zn2Ac. -C=O (1627 cm^{-1}), -C=N (1594 cm^{-1}), -C=C (1419 cm^{-1}).

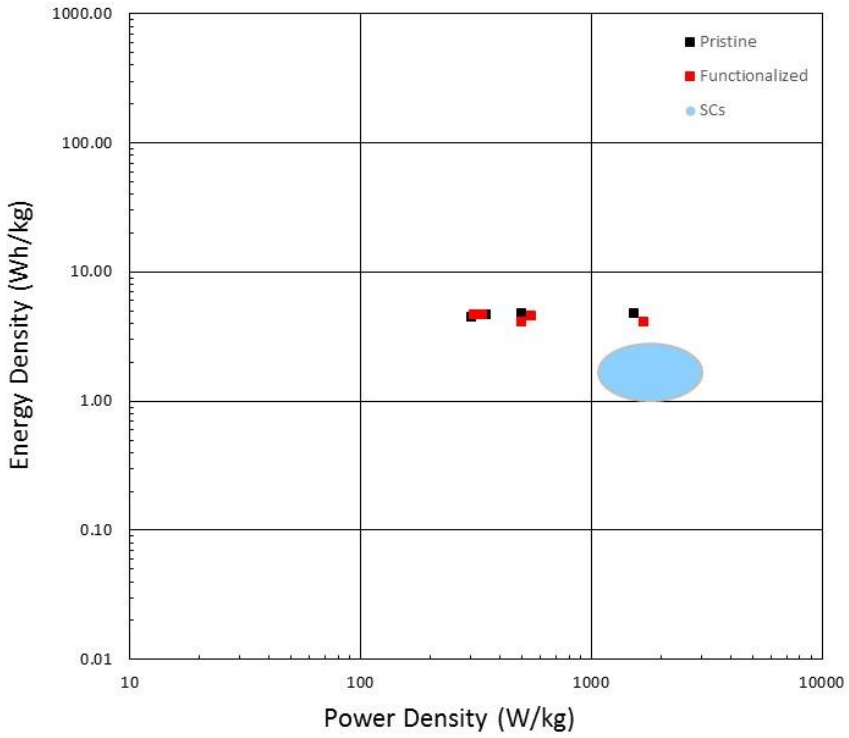

Figure S11: Ragone plot plotting energy density as a function of power density. Pristine and functionalized films are compared to commercially available supercapacitors. Energy density is not lost as power density is increased.

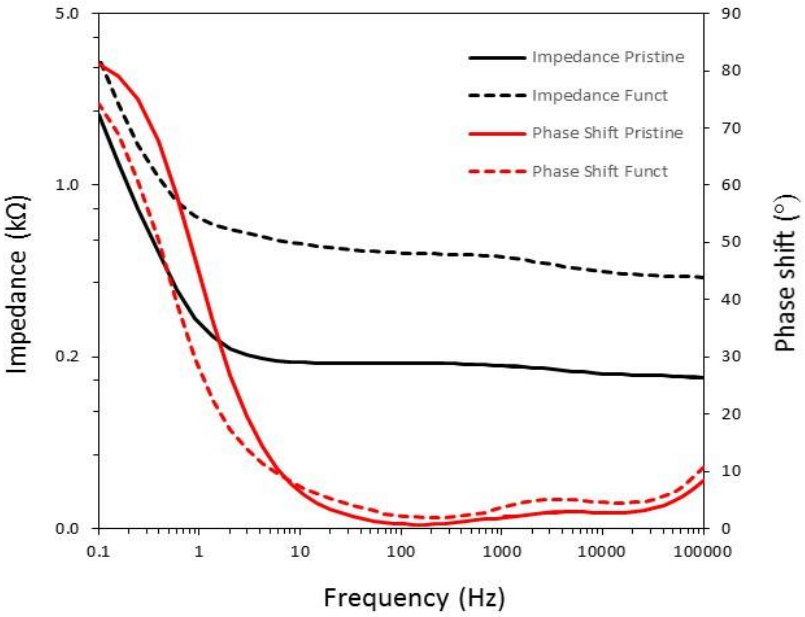

Figure S12A: EIS of pristine and functionalized SWCNTs with 20.2 and 20.4 μg of CNTs, respectively. The operating potential was 1 V with a current amplitude of 5 mV. Impedance through the functionalized film (420 Ω) was larger than pristine (250 Ω) .

For EIS, the average measured impedance of pristine SWCNTs was calculated as 260 ± 50 Ω at 1 V. As the frequency increased, the impedance of the system decreased. The functionalized film shows much larger impedance than the pristine film (660 vs. 190 Ω at 100 Hz). Working hypotheses are that molecular spacers (even at low concentration) are prohibiting current transport, or the uneven surface morphology of the film creates greater impedance. On average, measured at 1 V, the impedance for pristine CNTs was 250 ± 50 Ω. For functionalized, 420 ± 30 Ω was measured. Using a 95% confidence interval, the films are statistically different. The higher impedance through functionalized films compared to pristine films could also suggest molecular spacer intercalation between CNTs. If CNTs are more spread out, current wouldn't flow as easily resulting in an increase in resistance/impedance.

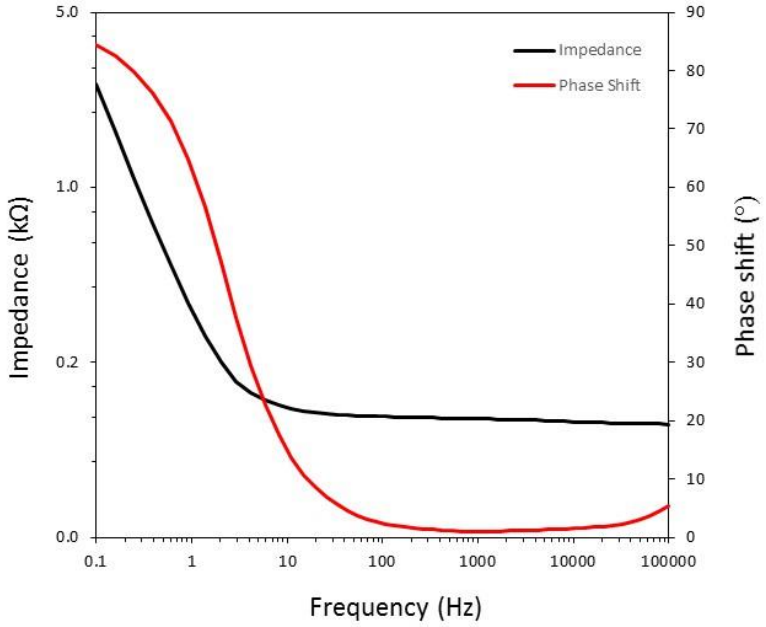

Figure S12B: EIS of pristine SWCNTs at 0 V with an amplitude of 5 mV. Average impedance for three films was calculated to be 260 ± 50 Ω. Reactance of the capacitive like behavior of SWCNTs shows a larger impedance at lower frequency.

Figure S13 – components to 13 mm syringe filter

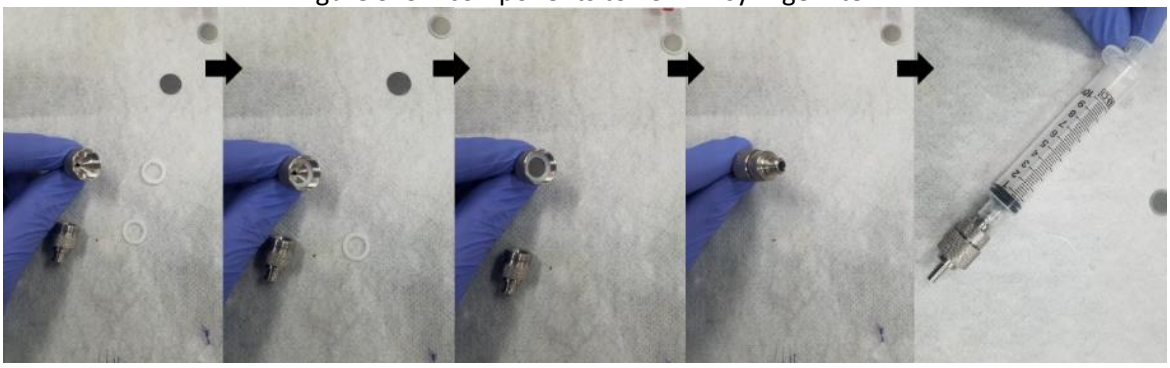

Figure S14 – 13 mm syringe assembly

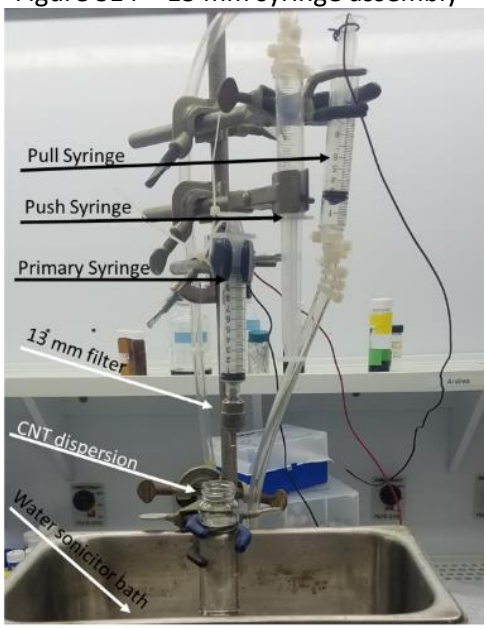

Figure S15 – Parts on auto cycle filter

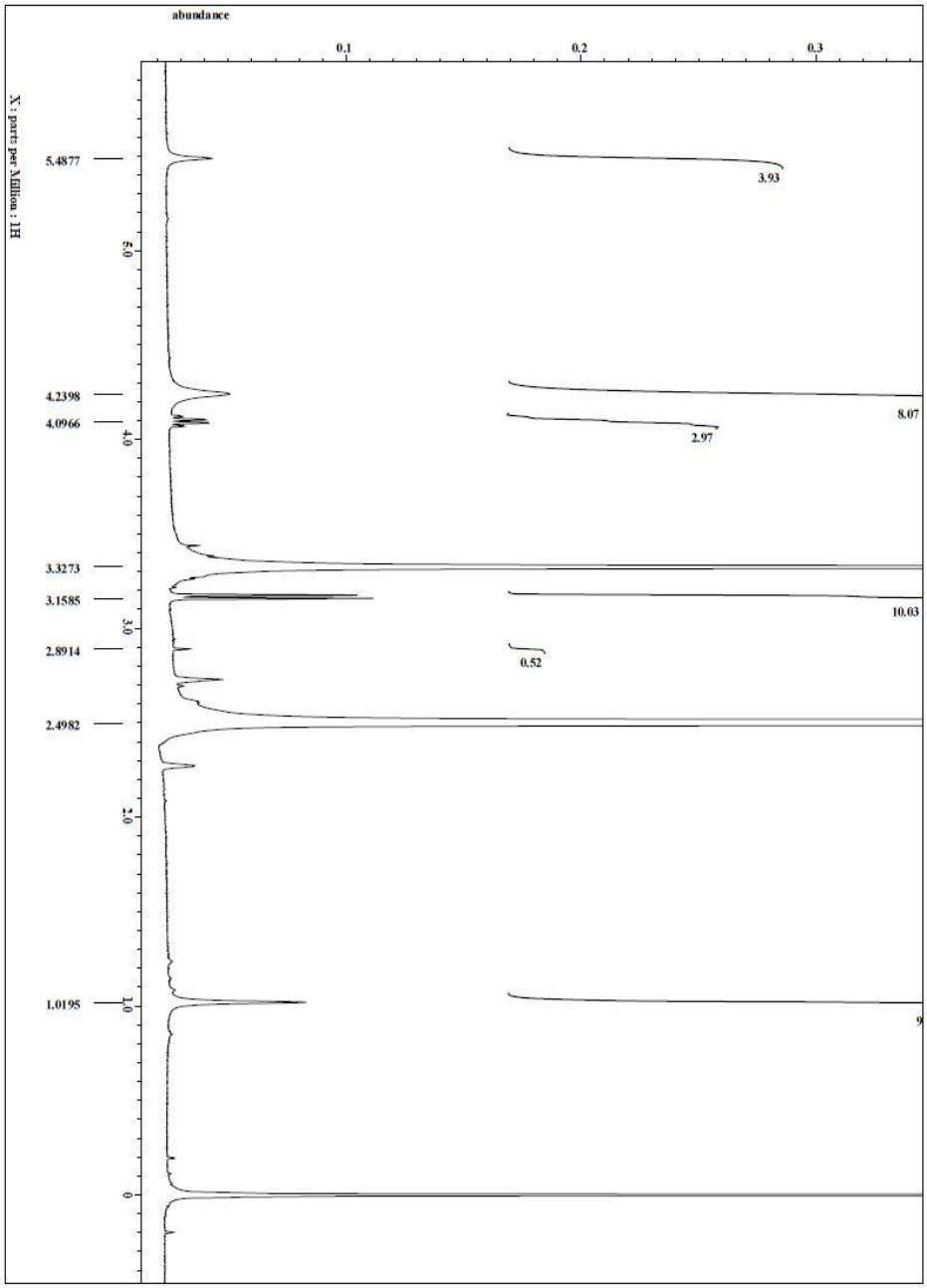

Figure S16: Proton NMR of Cu2FcOH. Shifts at 3.15 and 4.09 ppm are impurities in the sample. The –OH bridging ligand does not show a proton. The electron withdrawing effects of the metal centers could affect the shift significantly.

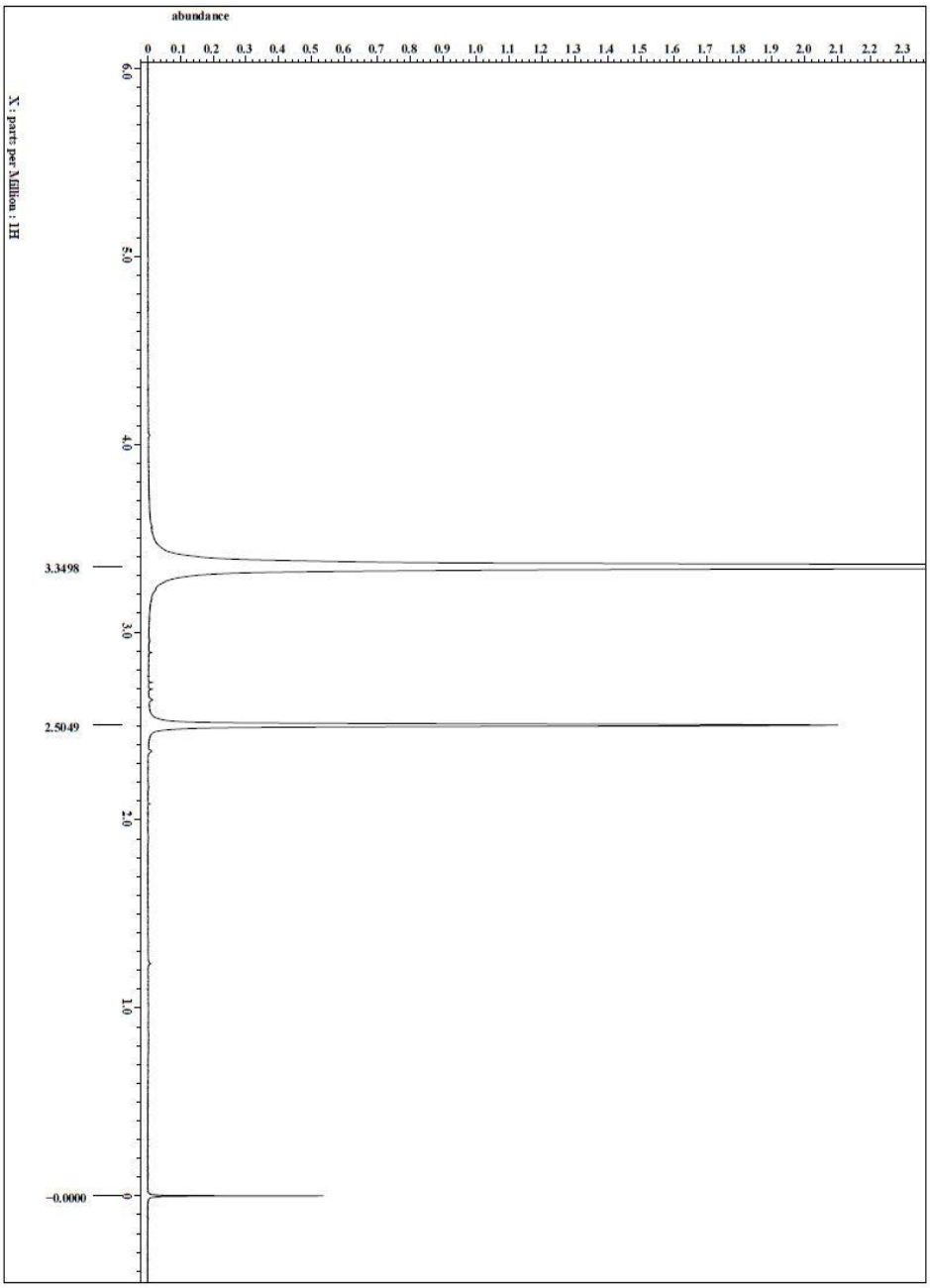

Figure S17: Proton NMR of Cu2FcCl3. The paramagnetic property of copper with the electron withdrawing chloro bridge can provide extreme deshielding of protons. However, no peaks are observed measured up to 200 ppm.

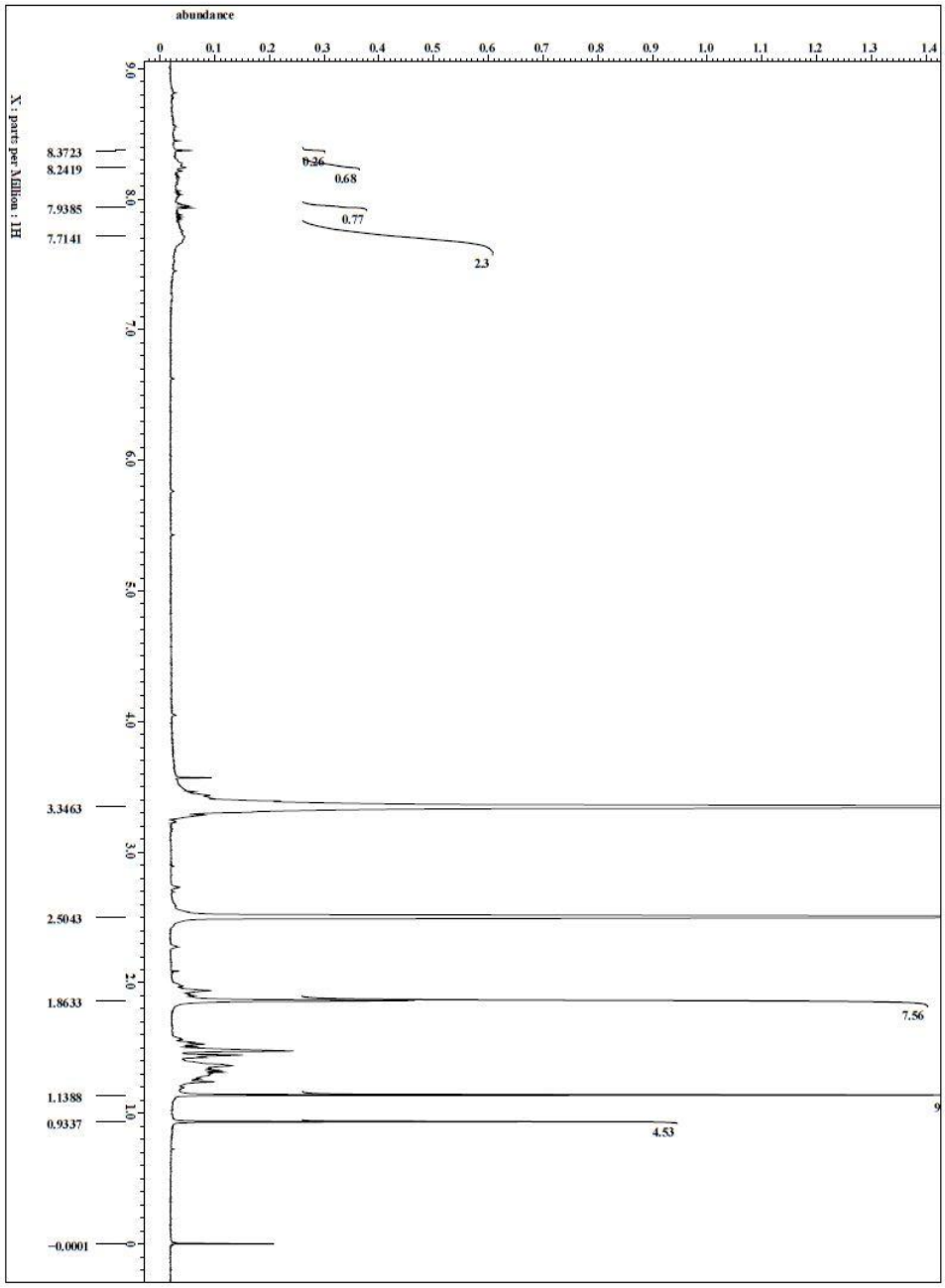

Figure S18: Proton NMR of +2Zn2Ac.

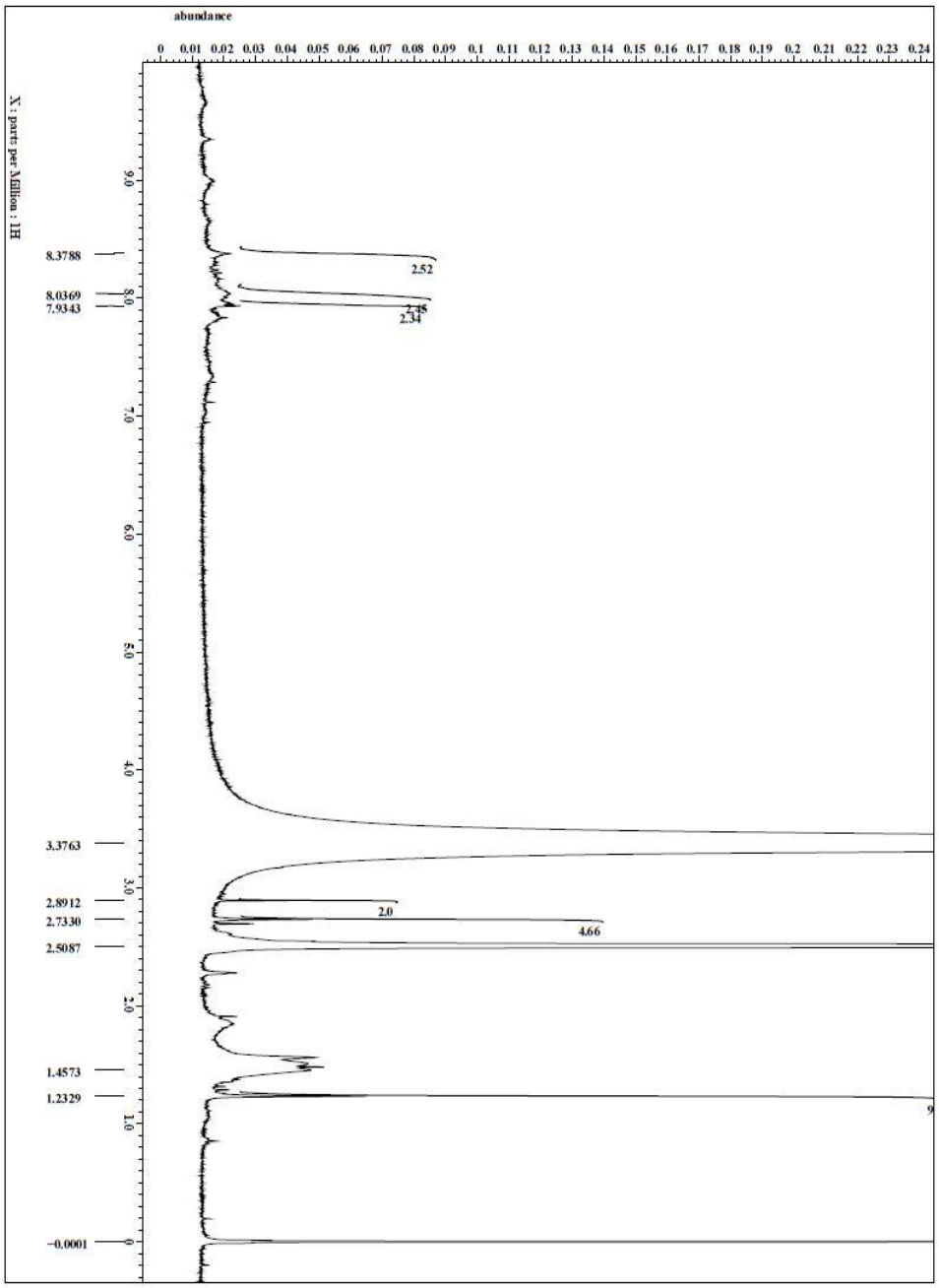

Figure S18: Proton NMR of +2Cu2

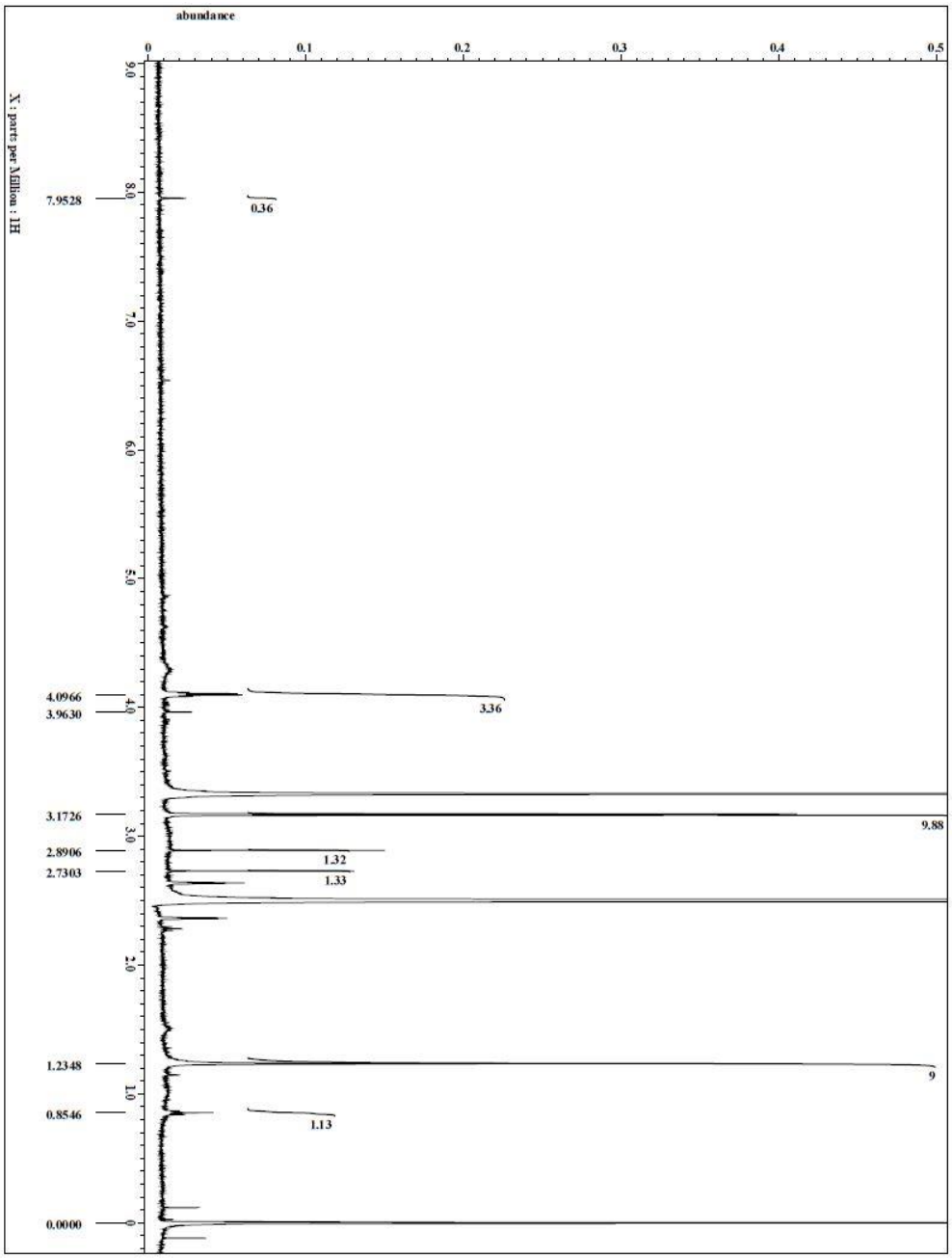

Figure S19: Proton NMR of +2Cu2FcOH. This shows a similar spectra to Cu2FcOH, which is expected due to the same structure minus a protonated nitrogen.

Electrical Characterization Equations:

$$C = \frac{\varepsilon_0 \varepsilon_r A}{d}$$

where C is capacitance in Farads, ε_0 is the dielectric constant of free space in vacuum, ε_r is the dielectric constant of the solvent in F m^{-1}, A is the surface area of the material in m^2, and d is the distance between electrical double layer and ion interface in m.

$$C = \frac{Q}{V}$$

where the capacitance in Farads is equal to the charge stored, Q divided by the potential at which the parallel-plate capacitor is maintained, V

Using GCD data we analyze C using the time derivative of Q = CV such that:

$$C = \frac{dQ/dt}{dV/dt}$$

Since $dQ/dt = I$ the constant current and dV/dt is measured from the experimental slope of the discharge curve. C_s = C/m where m is the mass of the active material in the working electrode.

Specific energy is calculated from the know equation $E_s = \frac{C_s \cdot (\Delta V)^2}{2}$ where ΔV is measured over the linear portion of discharge curve.

Specific power is calculated from the specific energy and the Δt measured during the discharge:

$$P_s = \frac{E_s}{\Delta t}$$